CHAPTER

9

Trans-Neptunian binaries (2018)

Keith S. Noll^a, William M. Grundy^b, David Nesvorný^c, Audrey Thirouin^b

^aGoddard Space Flight Center, Greenbelt, MD, United States ^bLowell Observatory, Flagstaff, AZ, United States ^cSouthwest Research Institute, Boulder, CO, United States

9.1 Overview

At the time of the Coimbra conference in early 2018 four decades had elapsed since the discovery of the first Trans-Neptunian binary (TNB) companion—Charon, almost two decades since the first discoveries of additional TNBs (e.g., Veillet et al., 2002), and 10 years since the last major review of this topic (Noll et al., 2008a). In this chapter, we start from the foundation of this earlier work and review new developments in the field that have occurred in the last decade.

In 2008, many of the themes relating to TNBs had already been established and the basic outlines of our current understanding of the Trans-Neptunian solar system and the role of binaries within that population had begun to take shape. Since that time there has been continued progress in the identification of binaries, determination of mutual orbits, and understanding of system mass, density, rotational state, component colors, and mutual events. Formation models have shifted away from capture scenarios in favor of models that invoke direct gravitational collapse—binaries offer tests of such models while also constraining subsequent dynamical evolution. In 2018, the study of TNBs remains one of the most active areas of progress in understanding the solar system beyond Neptune.

9.2 Inventory

9.2.1 Direct imaging

The discovery of new binaries has continued over the last decade, with the majority of new systems being discovered by the Hubble Space Telescope (HST) as was also true in the previous decade. At the time of the last review, 43 binary systems were known (Noll et al., 2008a); that number has now doubled to 86 Trans-Neptunian objects (TNOs) with one or more companions (see compilation¹ maintained by Johnston, 2018).

TNBs have been found in every dynamical population of the Kuiper belt as shown in Fig. 9.1. As discussed in more detail here, this includes a large number of binaries in the cold classical population (nonresonant, not scattering, and low inclination) and significant numbers also in the dynamically hot populations—that is, objects in mean-motion resonance with Neptune, objects that are scattered by Neptune, detached objects with large perihelia, and high inclination (hot) classicals (Elliot et al., 2005; Gladman et al., 2008). Large snapshot surveys with HST have historically been the most productive source of binary discovery accounting for approximately 80% of discoveries. Snapshot observations have been an efficient way to observe a significant number of solar system objects with HST; however, the reduced exposure times dictated by this observing strategy favored brighter objects and observations in a single broad filter. In the last decade, searches with HST have been focused more on follow-up of distinct subpopulations underrepresented in earlier surveys. Overall, HST has observed more than 500 TNOs, a significant fraction of the total Trans-Neptunian population with well-known orbits.

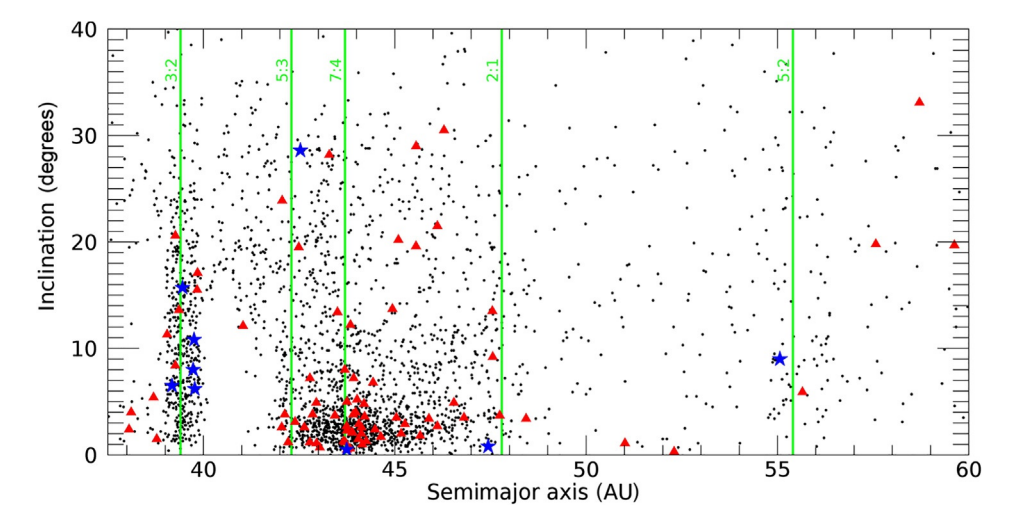


FIG. 9.1 TNOs with semimajor axes between 38 and 60 AU (*black points*) are shown in this plot of semimajor axis versus inclination. Resolved TNBs are shown as *red triangles* while possible contact binaries identified from light curve analysis are shown as *blue stars*.

¹ See http://www.johnstonsarchive.net/astro/asteroidmoons.html.

9.2 Inventory 207

9.2.2 Light curves

Light curve evidence for elongated bodies, close binaries, and/or bilobed objects (contact binaries) is found in most small body populations including near-Earth objects (Benner et al., 2015), main belt asteroids (Agarwal et al., 2017), trojans (Ryan et al., 2017), comets (Harmon et al., 2010; Nesvorný et al., 2018), and TNOs (Sheppard and Jewitt, 2004; Lacerda et al., 2014; Thirouin and Sheppard, 2017, 2018; Thirouin et al., 2014, 2017). For a subset of objects that are large and/or close enough to the Earth or a spacecraft direct imaging or radar data is available to confirm their bilobed/contact-binary shape. However, for the majority of objects with similar light curve signatures, the detailed shape is indeterminate. It is nevertheless clear that such objects are quite common across the solar system. The Trans-Neptunian population is no exception with early estimates of the fraction of such objects at about 30% (Sheppard and Jewitt, 2004; Lacerda, 2011).

Potential close/contact binaries in the Kuiper belt are not directly resolvable due to the small angular separation of the system's components but candidates can be identified by rotational light curves (Thirouin et al., 2017) or by occultations. In the case of the Plutino 2001 QG_{298} , Sheppard and Jewitt (2004) argued that the large 1.14 mag amplitude light curve coupled with the 13.77-hour (double-peaked) rotation period was incompatible with an equilibrium fluid body with the required axial ratio. They proposed instead that 2001 QG_{298} is a likely contact binary. The decreased amplitude of 0.7 mag observed in 2010 was compatible with the change in viewing geometry of a contact-binary-like system (Lacerda, 2011).

A second example of a TNO with a large light curve amplitude (0.85 mag) is 2003 SQ_{317} (Lacerda et al., 2014). This object is of special interest because it is a possible member of the Haumea collisional family. The authors noted the possibility of distinguishing between different hydrostatic equilibrium shape models by monitoring the light curve amplitude over multiple years, a technique that can separate elongated ellipsoids and contact-binary shapes given the right alignment and sufficient time baseline

Six additional contact-binary candidates have recently been identified from a survey using Lowell's Discovery Channel Telescope and the Magellan Telescope (Thirouin et al., 2017; Thirouin and Sheppard, 2017, 2018; Fig. 9.2). Preliminary estimates from this survey suggest that as many as \sim 40%–50% of Plutinos but only \sim 10%–25% of cold classicals are candidate contact binaries (Thirouin and Sheppard, 2019). This difference, if confirmed with larger numbers of objects, may be an important clue to the dynamical evolution of these populations.

Finally, although it is routine in the literature to refer to the objects we have described as candidate contact binaries, it is worth pointing out that light curves are insensitive to concavities and that even rubble piles have sufficient strength that they cannot be treated as hydrostatic fluid bodies (Harris and Warner, 2018). On the other hand, the contact-binary shape of the cold classical (486958) 2014 MU₆₉, first revealed by stellar occultation (Buie et al., 2019) and dramatically confirmed by the New Horizons fly-by (Porter et al., 2019) stands as an existence proof and strong validation of both indirect shape determination methods and the models that predict a plentitude of such binaries. The lack of a detectable light curve for this object (Benecchi et al., 2019) is a reminder that the light curve technique is sensitive to the pole orientation and that many other similar hidden binaries may exist. Continued investigation of the Trans-Neptunian contact-binary population promises to be a productive observational and theoretical enterprise.

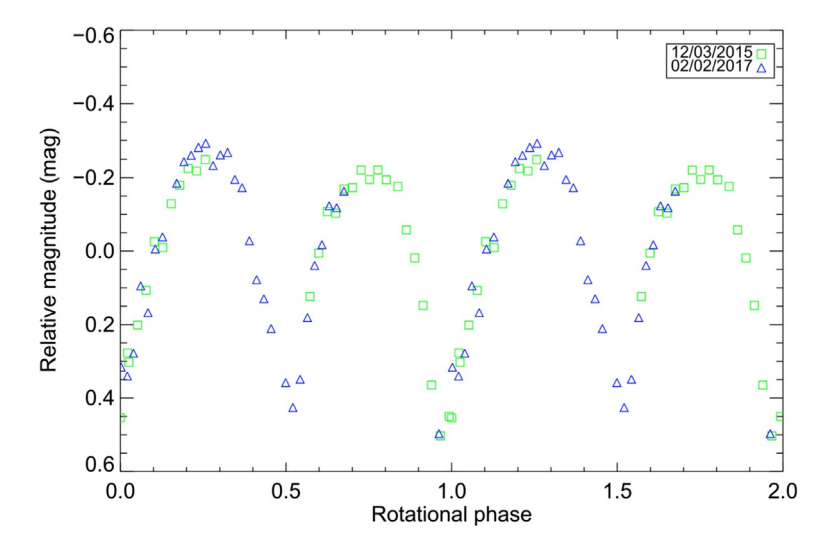


FIG. 9.2 The light curve of 2004 TT₃₅₇ shows a large amplitude and a narrow V-shaped minimum that is characteristic of highly elongated bodies including bilobed configurations. The rotational period of 7.79 hours rules out a hydrostatic fluid shape as a possible source of this elongation, leaving a "contact" binary as a possibility (Thirouin et al., 2017).

9.3 Binary frequency

One of the most frequently asked and seemingly simple questions about TNBs is what fraction of the population they represent. However, any such question must be qualified by knowledge of observational limitations and biases, possible differences between populations, possible size dependencies, knowledge of the separation distribution and regions of orbital stability as well other confounding factors. Any attempt to simply divide the number of detected companions by the number of objects observed will yield a result that is nearly devoid of significance. Following we explore some of the different aspects of determining binary frequency.

While the first TNBs were found from ground-based telescopic observations, the vast majority of known binaries have been discovered by HST (Noll et al., 2008a). Only a small fraction of known binaries are ever widely enough separated that they can be observed from ground-based telescopes without adaptive optics (AO), even in the best of seeing. And AO systems must use a laser guide star with stellar appulse because the targets are too faint for wavefront correction. HST detections have heterogeneous instrumental resolution and observational S/N that must be considered when attempting to estimate the frequency of binaries.

In addition to instrumental considerations, the heterogeneity of the sample itself must be considered. The angular size of the Hill sphere is independent of distance for objects with equal mass. But the wide range in albedo (Stansberry et al., 2008) and differing heliocentric eccentricities result in Hill radii that vary depending on an object's density, albedo, and orbit. The largest TNOs may retain volatile ices on their surfaces that can cause unusually

9.3 Binary frequency 209

high albedos. Among smaller TNOs, higher albedos are found among the cold classicals than among other dynamical classes (Brucker et al., 2009; Vilenius et al., 2012, 2014). Thus, magnitude-limited surveys will, in general, have a biased sensitivity to secondaries when comparing different classes of objects. We consider two different examples that illustrate issues in appropriately determining binary frequency.

9.3.1 Binary fraction in the cold classicals

One of the earliest published results on the binary fraction in the Kuiper belt populations was the observation that the fraction of binaries in the cold classical population appeared to be greater than that of the dynamically excited populations and, more specifically, the so-called hot classicals (Stephens and Noll, 2006; Noll et al., 2008b) which overlap the cold classicals in semimajor axis space, but have a higher inclination (Levison and Stern, 2001; Brown, 2001). This observation is one of a group of apparently unique features of the cold classicals that along with their color (Tegler and Romanishin, 2000) and the presence of wide binaries (Parker and Kavelaars, 2010) has been used to argue that the cold classicals are a relatively undisturbed remnant of the primordial planetesimal disk.

But the high binary fraction in the cold classicals is subject to a surprising complication that must be considered carefully. Fig. 9.3 plots 110 cold classicals ($i \le 5.5$ degrees) observed with HST in two different ways. When binned by the absolute magnitude of the unresolved system (i.e., the magnitude reported by ground-based discovery observations), there is a large excess of cold classical binaries for 6.15 > H > 4.95 mag (Noll et al., 2014). The hot classicals do not show a similar behavior. This effect can be understood as being due to the extreme steepness of the magnitude-frequency distribution (MFD) of the cold classicals (Fraser et al., 2014) resulting in the brightest objects being dominated by binaries. Because the observed targets are heavily biased to the brightest available members of the population, the apparent binary fraction can be magnified. However, even at fainter system magnitudes, H > 6.15 mag, the binary frequency among cold classicals is $\sim 20\%$ and exceeds that found in the hot classicals in the same magnitude range.

The higher albedo for cold classicals means that the mass of a cold classical is likely to be lower than a hot classical of the same absolute magnitude. Because the Hill radius scales with the system mass, the likelihood of finding a secondary at the same separation in terms of Hill radius is, therefore, lower for a cold classical than for a hot classical of the same absolute magnitude. Thus, the high fraction of cold classical binaries appears to be a robust feature of the population.

When the same data are plotted as a function of the absolute magnitude of the primary, there is no excess among the largest objects and the frequency is roughly constant down to $H \sim 8$ mag. Crudely debiasing by scaling all binaries to the faintest absolute magnitude bin and removing undetectable secondaries does not significantly alter this result. Although the dip from $H \sim 6.5-7.0$ appears significant, Nesvorný et al. (2011) used the lack of a sustained drop off at even fainter magnitudes to constrain collisional grinding among cold classicals. Further observations of cold classicals, especially fainter ones, are needed to better understand this structure.

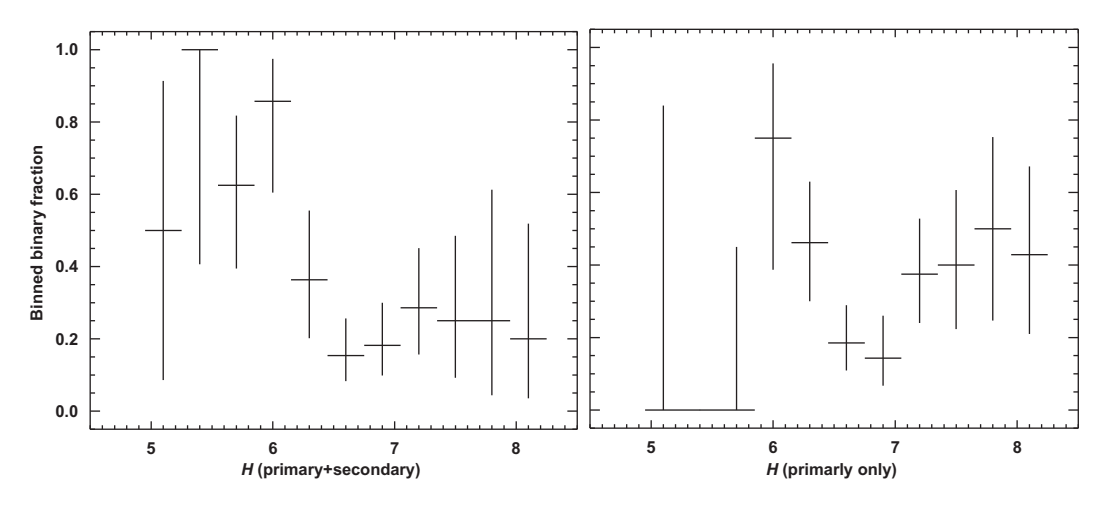


FIG. 9.3 The binned binary fraction of cold classical KBOs observed with HST is plotted as a function of the overall system magnitude (*left*) and by the brightness of the largest component (*right*). The large excess of binaries among the brightest systems (*left*) is the product of an extremely steep MFD that causes the brightest cold classicals to be dominated by near-equal mass binaries (Noll et al., 2014). When plotted by the magnitude of the largest component (*right*), the lack of a drop-off at faint magnitudes is evidence that the observed slope change in the MFD is not due to collisional grinding (Nesvorný et al., 2011).

9.3.2 Resonant binaries

Binaries found in dynamically excited populations, including hot classicals, scattered disk, and Resonant populations, are potentially diagnostic indicators of the dynamical perturbations experienced by these objects over their histories. Noll et al. (2012) examined binaries in populations in mean-motion resonance with Neptune where a total of 76 Plutinos and 96 objects in other resonances had been observed with HST. As shown in Fig. 9.4, the lack of binary Plutinos at low inclination is particularly striking, with a binary fraction of only 5^{+6}_{-2} % for i < 12 degrees and $5 \le H \le 8$ mag. In this same data set, there are no binary Plutinos with i < 5.5 degrees. This can be compared to 27^{+16}_{-9} % found for the 2:1 resonance with i < 12 degrees in the same absolute magnitude range, a value similar to that found for the cold classicals (29^{+7}_{-6} %). This result appears to be consistent with the predicted behavior of low-e migration of Neptune and coherent capture into resonances (Murray-Clay and Schlichting, 2011) if the 2:1 resonance swept over the cold classicals, but the 3:2 resonance did not.

9.4 Mutual orbits

Orbits of TNBs have mostly been obtained from multiepoch imaging with sufficiently high spatial resolution to separate the two objects. The widest binaries are separated by a few arcsec, and can be resolved even in natural seeing, but most are separated by much less, requiring AO or the HST.

9.4 Mutual orbits 211

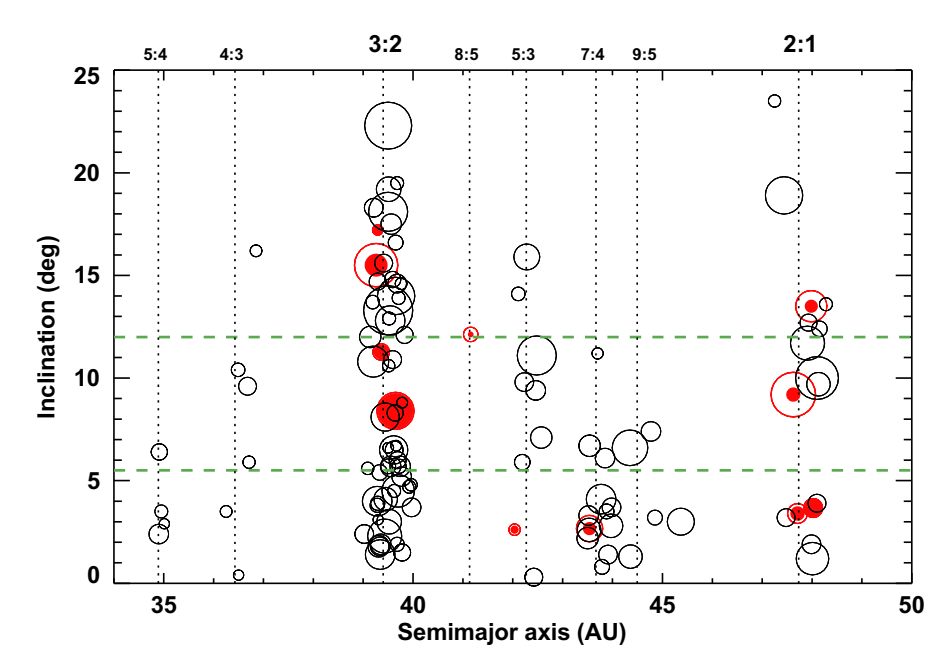


FIG. 9.4 Resonant Trans-Neptunians with absolute magnitudes $5 \le H \le 8$ mag observed by HST as of 2012 are shown by *circular symbols*. The size of the symbol scales inversely with absolute magnitude. Objects identified as binaries are shown in *red* with the primary represented by an *open circle* and the secondary shown as a *filled circle*. Resonances with identified objects are shown along the top of the figure. The *green dashed horizontal lines* at i = 5.5 degrees and i = 12 degrees mark two proposed "crossover" boundaries of the cold and hot classical inclination distributions. Objects captured by low-e resonance sweeping should have inclinations mostly below these bounds, as described in the text.

Resolved observations at four epochs can, in principle, determine the seven parameters required to fully describe a Keplerian binary orbit (total mass and six orbital elements), but in practice this is a function of how well the observations sample the orbit. The sampling can be improved by using the accumulating collection of data to optimize the timing of each subsequent observation (e.g., Grundy et al., 2008). The mirror ambiguity of an orbit projected onto the sky-plane can eventually be resolved through changing observation geometry, but it takes multiple years for sufficient parallax to accumulate. In some cases, the similarity in brightness between the two components makes it impossible to tell which of them is which from one epoch to the next—more observations are then required to yield a unique solution. Despite these complications, the last decade has seen significant progress. Of the 86 TNBs/multiples known, the orbit is fully known for 37. For 11 more, the period, semimajor axis, and eccentricity are known, but the sky-plane mirror ambiguity remains to be broken. These orbital parameters are collected in Table 9.1

TABLE 9.1 Mutual orbital parameters of TNBs.

	-						
Object	P (days)	a (km)	e	Incl. ^a (degrees)	M_{sys} (10 ¹⁸ kg)	a/r _H b	Refs.
26308 1998 SM ₁₆₅	130.154	11,374	0.4732	75.46	6.88	0.02425	Margot et al. (2004) and Grundy et al. (2011)
42355 Typhon—Echidna	18.9815	15 <u>8</u>	0.507	54	0.87	0.0115	Grundy et al. (2008) and Stansberry et al. (2012)
50000 Quaoar—Weywot	12.431	133 <u>3</u>	0.021	-	12 <u>1</u>	0.00364	Fraser et al. (2013) and Brown and Butler (2017)
55637 2002 UX ₂₅	8.3095	47 <u>5</u>	0.18	65.0	123	0.00314	Brown and Butler (2017) and Brown (2013)
58534 Logos—Zoe	309.9	82 <u>2</u>	0.546	74.2	0.458	0.0326	Margot et al. (2004), Grundy et al. (2011), and Noll et al. (2004b)
60458 2000 CM ₁₁₄	24.825	2500	0.03	56	2.00	0.00667	Grundy et al. (2019a)
65489 Ceto—Phorcys	9.560	18 <u>5</u>	0.008	_	5.5	0.0071	Grundy et al. (2007)
66652 Borasisi—Pabu	46.289	45 <u>3</u>	0.470	49.4	3.44	0.00916	Noll et al. (2004a)
79360 Sila—Nunam	12.51006	27 <u>7</u>	0.026	123.3	10.8	0.00351	Grundy et al. (2012)
88611 Teharonhiawako— Sawiskera	828.8	27, <u>6</u> 00	0.249	127.6	2.44	0.0581	Grundy et al. (2011) and Osip et al. (2003)
90482 Orcus—Vanth	9.53915	9000	0.0009	106.7	635	0.004311	Brown and Butler (2017), Grundy et al. (2019a), and Brown et al. (2010)
119979 2002 WC ₁₉	8.403	409	0.20	_	77	0.00329	Grundy et al. (2019a)
120347 Salacia—Actaea	5.49388	57 <u>2</u>	0.010	41.4	492	0.00233	Stansberry et al. (2012) and Grundy et al. (2019a)
123509 2000 WK ₁₈₃	30.913	23 <u>7</u>	0.014	_	1.10	0.00655	Grundy et al. (2011)
134860 2000 OJ ₆₇	22.0585	22 <u>7</u>	0.012	_	1.90	0.00523	Grundy et al. (2009)

136199 Eris—Dysnomia	15.78590	372 <u>7</u>	0.0062	78.5	16,4 <u>70</u>	0.004724	Grundy et al. (2011) and Brown and Schaller (2007)
148780 Altjira	139.56	9900	0.344	25.4	3.95	0.0182	Grundy et al. (2011)
160091 2000 OL ₆₇	347.1	7 <u>8</u> 00	0.24	-	0.32	0.035	Grundy et al. (2019a)
160256 2002 PD ₁₄₉	1675	26, <u>8</u> 00	0.588	21.9	0.54	0.099	Grundy et al. (2019a)
174567 Varda	5.7506	48 <u>1</u>	0.022	-	266	0.00232	Grundy et al. (2015)
229762 G!kún 'hòmdímà	11.3147	60 <u>4</u>	0.024	32.3	136	0.00383	Grundy et al. (2019b)
275809 2001 QY ₂₉₇	138.118	99 <u>6</u>	0.418	161.0	4.10	0.01855	Grundy et al. (2011, 2019a)
341520 Mors—Somnus	972.2	209 <u>9</u>	0.1494	24.3	0.776	0.0955	
							Sheppard et al. (2012)
$364171\ 2996\ JZ_{81}$	1500	3 <u>3</u> 00	0.85	11	1.3	0.090	Parker et al. (2011)
385446 Manwë	110.18	66 <u>7</u>	0.563	49.1	1.94	0.0167	Grundy et al. (2014)
469514 2003 QA ₉₁	10.1089	15 <u>9</u>	0.02	-	3.1	0.00318	Grundy et al. (2019a)
469705 Ką́gára	128.11	7 <u>7</u> 00	0.69	11.2	2.2	0.0178	Grundy et al. (2019a)
508788 2000 CQ ₁₁₄	220.48	69 <u>4</u>	0.095	44.4	0.545	0.0253	Grundy et al. (2019a)
508869 2002 VT ₁₃₀	30.761	30 <u>3</u>	0.019	-	2.3	0.0067	Grundy et al. (2019a)
1998 WW ₃₁	587.3	226 <u>2</u>	0.819	51.7	2.66	0.04839	Grundy et al. (2019a) and Veillet et al. (2002)
1999 OJ ₄	84.115	33 <u>1</u>	0.368	57.4	0.405	0.01448	Grundy et al. (2009, 2019a)
1999 RT ₂₁₄	126.50	3400	0.30	23	0.19	0.0179	Grundy et al. (2019a)
2000 CF ₁₀₅	3 <u>9</u> 00	34 <u>,3</u> 00	0.33	-	0.22	0.166	Parker et al. (2011)
2000 QL ₂₅₁	56.449	49 <u>9</u>	0.489	134.1	3.09	0.01097	Grundy et al. (2009, 2019a)

Continued

9.4 Mutual orbits

TABLE 9.1 Mutual orbital parameters of TNBs—cont'd

Object	P (days)	a (km)	e	Incl. ^a (degrees)	M_{sys} (10 ¹⁸ kg)	a/r _H ^b	Refs.
2001 QC ₂₉₈	19.2287	38 <u>1</u>	0.334	73.7	11.9	0.00502	Margot et al. (2004) and Grundy et al. (2011)
2001 QW ₃₂₂	62 <u>8</u>	102, <u>1</u> 00	0.464	152.8	2.14	0.223	Parker et al. (2011)
2001 XR ₂₅₄	125.58	93 <u>1</u>	0.556	21.1	4.06	0.01687	Grundy et al. (2009, 2019a)
2002 XH ₉₁	371.1	22 <u>,4</u> 00	0.71	39	6.5	0.0359	Grundy et al. (2019a)
2003 QY ₉₀	309.6	85 <u>5</u>	0.663	51.4	0.52	0.0320	Grundy et al. (2011)
2003 TJ ₅₈	137.68	38 <u>3</u>	0.516	63	0.236	0.0187	Grundy et al. (2011, 2019a)
2003 UN ₂₈₄	31 <u>8</u>	5 <u>4</u> 00	0.38	23.0	1.27	0.145	Parker et al. (2011)
2004 PB ₁₀₈	97.020	10,400	0.438	83.2	9.5	0.0148	
							Grundy et al. (2009, 2019a)
2005 EO ₃₀₄	3 <u>6</u> 00	6 <u>9</u> 00	0.21	_	2.0	0.155	Parker et al. (2011)
2006 BR ₂₈₄	1500	25 <u>,4</u> 00	0.275	54.1	0.576	0.0884	Parker et al. (2011)
2006 CH ₆₉	14 <u>2</u>	2 <u>7</u> 00	0.896	133	0.8	0.081	Parker et al. (2011)

^aInclination between the mutual orbit and the heliocentric orbit, where known.

bSemimajor axis in units of Hill radii, a measure of how tightly bound the orbit is.

CThe first uncertain decimal in each figure is either underlined or the last decimal shown.

9.5 Properties derived from orbits

9.5.1 Mass and density

The total mass of a binary system can be calculated once the period and semimajor axis of the binary orbit are known. Mass is a fundamental property, providing valuable constraints on dynamics, as well as composition and internal structure, via the bulk density computed by dividing the mass by the estimated total volume of the bodies in the system. Object sizes, necessary to derive density, have been challenging to obtain. Observations at thermal infrared wavelengths can constrain radii to about $\pm 10\%$ precision, translating to a $\pm 30\%$ uncertainty in volume and density. As shown in Fig. 9.5, TNBs with system masses, $M_{\rm sys}$, of $\sim 10^{19} \, \rm kg$ and less, corresponding roughly to component diameters of $d < 300 \,\mathrm{km}$, have very low densities, mostly less than $100 \,\mathrm{kg}\,\mathrm{m}^{-3}$. More massive objects, $M_{sys} > 10^{21} \,\mathrm{kg}$, $d > 900 \,\mathrm{km}$ have higher densities, generally greater than 1500 kg m⁻³. In between, diverse densities are seen among the mid-sized bodies. Brown (2013) argued that the objects in the 300-900-kmdiameter-size range are too large to have retained much internal porosity, and suggested that their lower densities result from predominately ice-rich compositions, with more rock-rich compositions in the larger bodies accounting for their higher densities. However, a plot of density versus mass (Fig. 9.5) shows a consistent trend suggesting that a gradual reduction in pore space with increasing mass can explain the variation in density without resorting to ad hoc assumptions about composition. Looking ahead, stellar occultations enabled by the GAIA astrometric catalog have the potential to provide much more accurate sizes, and consequently better densities that will allow more detailed study of the densities of TNBs.

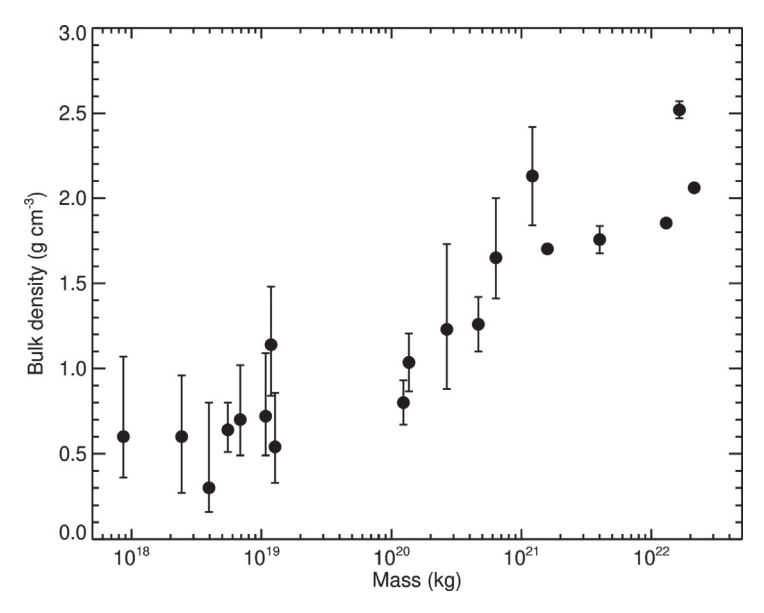


FIG. 9.5 Densities of TNOs versus mass show a smooth increasing trend over the $10^{19}-10^{22}$ kg mass range. (Triton and Charon are included because they fall in this mass range and have well-determined densities.)

9.5.2 Orbital eccentricity, inclination, and separation

The orbital properties of binaries can provide information about their formation circumstances as well as their subsequent dynamical evolution. For instance, circular orbits occur mostly among tightly bound binaries (Fig. 9.6), which is not a surprise, since these are the systems most prone to tidal evolution. Wide binaries with appreciable inclinations between their mutual orbits and heliocentric orbits are subject to the Kozai-Lidov effect (Kozai, 1962; Lidov, 1962) where the gravity of the distant Sun perturbs the mutual orbit, causing an oscillation between e and i. Grundy et al. (2011) argued that the broad peak of eccentricities around e = 0.5 was consistent with a population undergoing these oscillations. Because wide binaries are easier to discover and characterize than tight ones, it is likely that the tight circular orbits are underrepresented among the known orbits relative to the wider more eccentric ones.

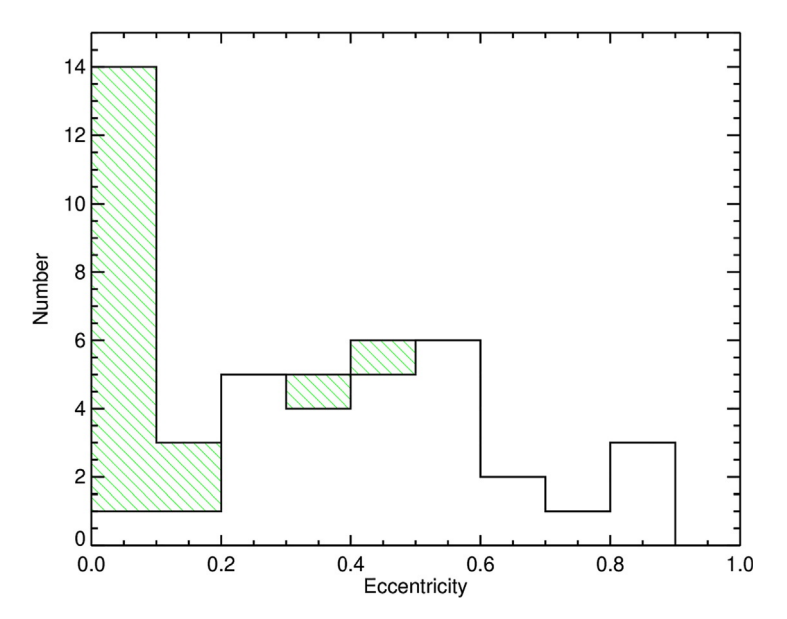


FIG. 9.6 Distribution of eccentricities of known binary orbits. Close binaries, that is, those with $a/r_H < 0.1$, are indicated by *green* hatching. Only one of the nearly circular orbits (e < 0.1) is not a close binary. At higher eccentricities most binaries are wider, although four close binaries also have eccentricities higher than 0.1.

The observation that there are considerably more prograde orbits than retrograde ones (Fig. 9.7; Grundy et al., 2009, 2011) is contrary to expectation from various capture scenarios (e.g., Goldreich et al., 2002; Schlichting and Sari, 2008; Kominami et al., 2011) that favor retrograde orbits, or, at most equal proportions of the two. Collisions should also not produce an excess of prograde systems Gravitational collapse from locally concentrated regions of the nebula, however, might preferentially produce prograde binaries (Nesvorný et al., 2010; Grundy et al., 2019a).

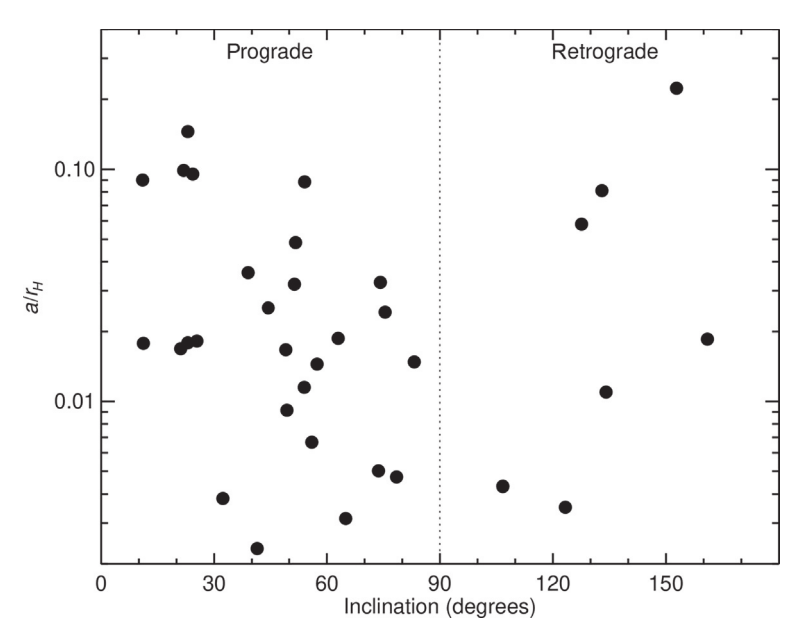


FIG. 9.7 Prograde orbits vastly outnumber retrograde orbits, except among the widest binaries. There is also a shortage of inclinations near 90 degrees among the wider binaries.

The widest binaries, those with a/r_H greater than about 0.05, do not show a strong prograde-retrograde asymmetry but do lack orbits with inclinations near 90 degrees. These highly inclined orbits are the ones that undergo the largest amplitude Kozai oscillations, leading to times of especially high eccentricity that could accelerate tidal evolution (e.g., Perets and Naoz, 2009; Naoz et al., 2010; Porter and Grundy, 2012), converting them into much tighter binaries, or perhaps leading to their becoming unbound.

A plot of a/r_H versus the excitation of the heliocentric orbit shows that most of the TNBs on more perturbed orbits are tightly bound (Fig. 9.8). This may be because the process of perturbing them into their present-day heliocentric orbits also dissociated most of the less tightly bound binaries. An exception is Mors-Somnus, a 3:2 resonant object (Sheppard et al., 2012) that is also a wide binary. Its existence suggests that nondestructive paths to excited heliocentric orbits, such as resonance sweeping, may have affected TNO populations.

9.5.3 Mutual events and occultations

Two additional channels for obtaining physical information that have begun to be exploited are mutual events and occultations. Mutual events occur twice in each TNB orbit when the binary orbit plane and the line of sight to Earth are nearly aligned. The duration of the individual mutual events and mutual event season depend on the particulars of the binary orbit, but are on the order of hours for individual events and approximate years for the season. With >40 TNB orbits known, it is reasonable to expect that one or two TNBs will have observable mutual events per decade.

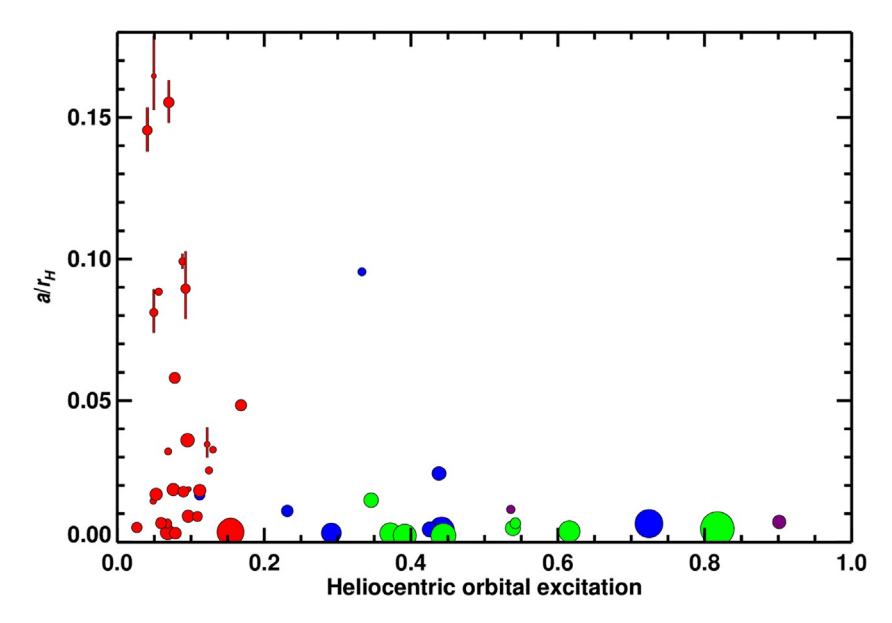


FIG. 9.8 Binary orbital looseness, as measured by a/r_H , versus the excitation of the heliocentric obit, as measured by $\sqrt{\sin(i_\odot)^2 + e_\odot^2}$, where i_\odot and e_\odot are the inclination and eccentricity of the heliocentric orbit. Colors indicate dynamical class: red for classical TNOs in low eccentricity, low inclination orbits, blue for objects in mean-motion resonance with Neptune, and green for scattered disk objects. The two purple objects are Centaurs, effectively scattered disk objects that have been perturbed into short-lived orbits crossing those of one or more of the giant planets.

Mutual events of the binary (79360) Sila-Nunam were predicted by Grundy et al. (2012). Benecchi et al. (2014) successfully observed one such event in February 2013 from multiple telescope facilities. Grundy et al. (2014) also predicted mutual events for (385446) Manwë-Thorondor in 2015–17. Attempts to observe Manwë-Thorondor with the SOAR telescope in August 2016 were reported by Rabinowitz et al. (2016), but final analysis remains pending. Fabrycky et al. (2008) and Ragozzine and Brown (2009) described a series of mutual events involving Haumea and one of its satellites, Namaka and attempted to observe one event using HST. Results of this observation were inconclusive. Fully realizing the potential of TNB mutual events will require more significant investments of large telescope observing time than has been available up to now.

Occultations by TNBs are another avenue of study that has only begun to be exploited. Sickafoose et al. (2019) report a ground-based occultation of Vanth, the satellite of Orcus, leading to diameter determination of 443 ± 10 km assuming a spheroidal body. The occultation-derived contact-binary shape of (486958) 2014 MU₆₉ (Buie et al., 2019) is another poignant example of the potential of occultation observations. The availability of precise stellar astrometric data from Gaia (e.g., Brown et al., 2018) promises to greatly expand the opportunities for similar observations in the future.

9.7 Formation scenarios 219

9.6 Colors

One of the most significant results to emerge from the study of TNBs has been the near identity of component colors (Noll et al., 2008a; Benecchi et al., 2009). This identity coupled with the wide range of colors of TNBs puts strong constraints on both formation mechanisms and subsequent color evolution. Capture models are limited to homogeneous regions and/or times within the larger potential color range seen in the current Kuiper belt. Subsequent physical evolution is also limited; in particular, nondisruptive collisions do not appear to result in color changes which would be seen as rotational color variability and/or variations in component colors.

Exceptions to binary component color identity among the largest TNOs and their satellites are attributable to highly volatile ices that are retained on the larger body, but are not stable on smaller components (e.g., Parker et al., 2016). More generally, it is possible that the satellites of the largest TNOs may have originated from impacts (e.g., Leinhardt et al., 2010), rather than by coaccretion or similar coformation mechanisms (see Section 9.6) and thus could have more global compositional differences.

Sheppard et al. (2012) noted that the wide Plutino binary, Mors-Somnus, has a very red color and argued for capture from the cold classical population based on the combination of this color and the near-equal component sizes. Fraser et al. (2017) used a similar color-based argument to leverage the neutral colors of several wide cold classical binaries into a more global conclusion on the compositional segregation of the protoplanetary disk and the ubiquity of binaries. However, the wide range of colors found in all Trans-Neptunian populations (e.g., Peixinho et al., 2015) greatly limits the use of color as an identifier capable of linking an individual object to a parent population. A much larger data set will be required in order to test these and similar ideas.

9.7 Formation scenarios

TNBs are an important tracer of planetesimal formation in the outer solar system and understanding how binaries formed is a critical test of planetesimal formation models. For example, if formed by capture (e.g., Goldreich et al., 2002), they constrain the dynamical conditions in the early protoplanetary disk (Schlichting and Sari, 2008). However, as noted earlier, the matching colors of binary components and prograde orbital orientations argue against this formation model.

An appealing alternative is a model in which planetesimals formed by the streaming instability (SI; Youdin and Goodman, 2005). The results of detailed hydrodynamical simulations (Johansen et al., 2009; Simon et al., 2017; Li et al., 2018) show that the SI clumps become gravitationally bound and result in a characteristic planetesimal size of \sim 100 km (depending on the details of disk parameters; Johansen et al., 2009).

The existing SI simulations also indicate that the collapsing clouds have vigorous rotation and their initial angular momentum typically exceeds, by a large margin, that of a critically rotating Jacobian ellipsoid with density $\rho=1000\,\mathrm{kg\,m^{-3}}$. This large excess of angular momentum that must be lost can produce a binary (Nesvorný et al., 2010, hereafter NYR10) with most of the angular momentum being deposited into the binary orbit.

NYR10 studied the collapse stage and Fig. 9.8 summarizes some results of the gravitational collapse. Equal-size KBO binaries ($R_2/R_1 > 0.5$, where R_1 and R_2 are the radii of primary and secondary components) form in the simulations if the initial clumps contract below the Hill radius ($R \le 0.6 R_H$) and/or have fast rotation ($\omega \ge 0.5 \omega_c$). This is roughly consistent with the results of the SI simulations where the clumps are small $R \sim 0.1 R_H$ and rotate as fast as they could. The gravitational collapse simulations also predict large separations between binary components (~ 1000 to $\sim 10^5$ km) and a broad distribution of binary eccentricities. Depending on the local disk conditions, the gravitational collapse may be capable of producing up to 100% binary fraction (for $\omega \ge 0.5\omega_c$). Because the binary components form from the local composition mix, the components should have identical compositions and colors, consistent with observations (see Section 9.5).

Another argument can be based on the inclination distribution of binary orbits (see Section 9.4). The SI simulations can be used to extract the orientation of the angular momentum vectors of individual clumps. NYR10 showed that the initial angular momentum vectors are a good proxy for the final orientation of binary orbits, allowing the SI results to be directly compared with observed binary orbits (Table 9.1); the results show a strikingly good match (Fig. 9.9).

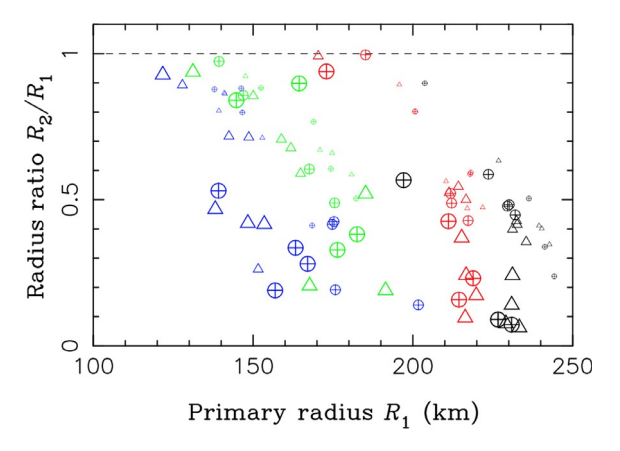


FIG. 9.9 The plot shows the sizes of binary components obtained in 96 simulations of gravitational collapse. Different initial conditions were used in each of these simulations. The initial rotation was assumed to be prograde (*triangles*) or retrograde (*crossed circles*) with respect to the orbital motion. The initial size of clumps, R, was set to be a fraction of the Hill radius at 30 AU, R_H (0.4, 0.6, and 0.8 R_H as indicated by the symbol size). The initial rotation was assumed to be a fraction of the critical frequency Ω_c (see NYR10 for definition): 0.1 (*black*), 0.25 (*red*), 0.5 (*green*), and 0.75 Ω_c (*blue*). For each setup, we performed four different simulations with slightly altered distributions of $N=10^5$ superparticles.

9.8 Future observations and summary

The entire field of study of Trans-Neptunian space stands on the cusp of a major revolution in data availability to be brought about by new surveys that will greatly expand the number of known TNOs. Because these surveys will be carried out by ground-based telescopes with

References 221

limited angular resolution, a proportionally large jump in the number of known binaries will come about as well, but more slowly as the result of painstaking follow ups with advanced AO or space-based telescopes. More binary orbits will also be determined, both from already-known binaries and yet-to-be discovered systems. Taken in whole on the timescale of the next decade, these developments promise improved statistics that will bring some of the conclusions reached so far into sharper focus.

Perhaps the greatest potential for the study of TNBs lies in the further observations of TNO light curves and of stellar occultations. Both of these techniques make it possible to explore close-in binaries—a population that cannot be reached by direct imaging. These efforts should be bolstered by the incontrovertible evidence delivered by the New Horizons mission that a heretofore underappreciated population of primordial binary objects awaits our study.

Finally, the expansion of our understanding of TNBs opens the door to comparisons with other related population including the Jupiter and Neptune Trojans, Centaurs, and comets. At least one of the targets of the Lucy mission, the Patroclus-Menoetius binary, has properties that look very much like those of many of the known TNBs (e.g., Buie et al., 2015). Answering whether this signals a genetic link or is simply a matter of chance will rely both on spacecraft data and a deep understanding of the binary populations of the outer solar system.

Acknowledgments

William M. Grundy and Keith S. Noll gratefully acknowledge support from the National Aeronautics and Space Administration (NASA)/ESA Hubble Space Telescope programs 13404, 13668, 13692, and 15233. Support for these programs was provided by the NASA through grants from the Space Telescope Science Institute, operated by the Association of Universities for Research in Astronomy, Inc. under NASA contract NAS 5-26555. Additional support was provided to William M. Grundy through NASA Keck PI Data Awards, administered by the NASA Exoplanet Science Institute. David Nesvorný's work is supported by NASA's Emerging Worlds. Audrey Thirouin is partly supported by the National Science Foundation, grant number AST-1734484. Audrey Thirouin also acknowledges Scott Sheppard for his contribution to the contact-binary search and characterization.

References

Agarwal, J., Jewitt, D., Mutchler, M., Weaver, H., Larson, S., 2017. A binary main-belt comet. Nature 549, 357.

Benecchi, S.D., Noll, K.S., Grundy, W.M., Buie, M.W., Stephens, D.C., Levison, H.F., 2009. The correlated colors of Trans-Neptunian binaries. Icarus 200, 292–303.

Benecchi, S.D., Noll, K.S., Thirouin, A., Ryan, E., Grundy, W.M., Verbiscer, A., et al., 2014. The UT 7/8 February 2013 Sila-Nunam mutual event Spiandspi future predictions. Icarus 229, 423–427.

Benecchi, S.D., Porter, S., Buie, M.W., Zangari, A.M., Verbiscer, A.J., Noll, K.S., et al., 2019. The HST lightcurve of (486958) 2014 MU₆₉. Icarus (in press). https://doi.org/10.1016/j.icarus.2019.01.023.

Benner, L.A.M., Busch, M.W., Giorgini, J.D., Taylor, P.A., Margot, J.L., 2015. Radar observations of near-Earth and main-belt asteroids. In: Michel, P., DeMeo, F.E., Bottke, W.F. (Eds.), Asteroids IV. University of Arizona Press, Tucson, AZ, pp. 165–182.

Brown, M.E., 2001. The inclination distribution of the Kuiper belt. Astron. J. 121, 2804–2814.

Brown, M.E., 2013. The density of mid-sized Kuiper belt object 2002 UX₂₅ and the formation of the dwarf planets. Astrophys. J. Lett. 778, L34.1-5.

Brown, M.E., Butler, B.J., 2017. The density of mid-sized Kuiper belt objects from alma thermal observations. Astron. J. 154, 19.1-7.

Brown, M.E., Schaller, E.L., 2007. The mass of dwarf planet Eris. Science 316, 1585.

- Brown, M.E., Ragozzine, D., Stansberry, J., Fraser, W.C., 2010. The size, density, and formation of the Orcus-Vanth system in the Kuiper belt. Astron. J. 139, 2700–2705.
- Brown, A.G.A., Vallenari, A., Prusti, T., de Bruijne, H.J., Babusiaux, C., Bailer-Jones, C.A.L., et al., 2018. Gaia data release 2: summary of the contents and survey properties. Astron. Astrophys. 616, A1.
- Brucker, M.J., Grundy, W.M., Stansberry, J.A., Spencer, J.R., Sheppard, S.S., Chiang, E.I., Buie, M.W., 2009. High albedos of low inclination classical Kuiper belt objects. Icarus 201, 284–294.
- Buie, M.W., Olkin, C.B., Merline, W.J., Walsh, K.J., Levison, H.F., Timerson, B., et al., 2015. Size and shape from stellar occultation observations of the double Jupiter trojan Patroclus and Menoetius. Astron. J. 149, 113.
- Buie, M.W., Porter, S.B., Tamblyn, P., Terrell, D., Verbiscer, A.J., Keeney, B., et al., 2019. Stellar occultation results for (486958) 2014 MU₆₉: a pathfinding effort for the new Horizons flyby. In: 50th Lunar and Planetary Science Conference, The Woodlands, Texas, ID 3120.
- Elliot, J., Kern, S.D., Clancy, K.B., Gulbis, A.A.S., Millis, R.L., Buie, M.W., et al., 2005. The deep ecliptic survey: a search for Kuiper belt objects and centaurs. II. Dynamical classification, the Kuiper belt plane, and the core population. Astron. J. 129, 1117–1162.
- Fabrycky, D.C., Ragozzine, D., Brown, M.E., Holman, M.J., 2008. Mutual events of (136108) 2003 EL₆₁ and S/2005 (136108) 2. Int. Astron. Union Circ. 8949, 1.
- Fraser, W.C., Batygin, K., Brown, M.E., Bouchez, A., 2013. The mass, orbit, and tidal evolution of the Quaoar-Weywot system. Icarus 222, 357–363.
- Fraser, W.C., Brown, M.E., Morbidelli, A., Parker, A., Batygin, K., 2014. The absolute magnitude distribution of Kuiper belt objects. Astrophys. J. 742, 100F.
- Fraser, W.C., Bannister, M.T., Pike, R.E., Marsset, M., Schwamb, M.E., Kavelaars, J.J., et al., 2017. All planetesimals born near the Kuiper belt formed as binaries. Nat. Astron. 1, 0088.
- Gladman, B., Marsden, B.G., VanLaerhoven, C., 2008. Nomenclature in the outer solar system. In: Barucci, M.A., Boehnhardt, H., Cruikshank, D.P., Morbidelli, A. (Eds.), The Solar System Beyond Neptune. University of Arizona Press, Tucson, AZ, pp. 43–57.
- Goldreich, P., Lithwick, Y., Sari, R., 2002. Formation of Kuiper-belt binaries by dynamical friction and three-body encounters. Nature 420, 643–646.
- Grundy, W.M., Stansberry, J.A., Noll, K.S., Stephens, D.C., Trilling, D.E., Kern, S.D., Spencer, J.R., Cruikshank, D.P., Levison, H.F., 2007. The orbit, mass, size, Albedo, and density of (65489) Ceto/Phorcys: a tidally-evolved binary centaur. Icarus 191, 286–297.
- Grundy, W.M., Noll, K.S., Virtanen, J., Muinonen, K., Kern, S.D., Stephens, D.C., et al., 2008. (42355) Typhon Echidna: scheduling observations for binary orbit determination. Icarus 197, 260–268.
- Grundy, W.M., Noll, K.S., Buie, M.W., Benecchi, S.D., Stephens, D.C., Levison, H.F., 2009. Mutual orbits and masses of six transneptunian binaries. Icarus 200, 627–635.
- Grundy, W.M., Noll, K.S., Nimmo, F., Roe, H.G., Buie, M.W., Porter, S.B., et al., 2011. Five new and three improved mutual orbits of transneptunian binaries. Icarus 213, 678–692.
- Grundy, W.M., Benecchi, S.D., Rabinowitz, D.L., Porter, S.B., Wasserman, L.H., Skiff, B.A., et al., 2012. Mutual events in the cold classical transneptunian binary system Sila and Nunam. Icarus 220, 74–83.
- Grundy, W.M., Benecchi, S.D., Porter, S.B., Noll, K.S., 2014. The orbit of transneptunian binary Manwë and Thorondor and their upcoming mutual events. Icarus 237, 1–8.
- Grundy, W.M., Porter, S.B., Benecchi, S.D., Roe, H.G., Noll, K.S., Trujillo, C.A., Thirouin, A., Stansberry, J.A., Barker, E., Levison, H.F., 2015. The mutual orbit, mass, and density of the large transneptunian binary system Varda and Ilmarë. Icarus 257, 130–138.
- Grundy, W.M., Noll, K.S., Roe, H.G., Buie, M.W., Porter, S.B., et al., 2019a. Mutual orbit orientations of transneptunian binaries. Icarus (in press). https://doi.org/0.1016/j.icarus.2019.03.035.
- Grundy, W.M., Noll, K.S., Buie, M.W., Benecchi, S.D., Ragozzine, D., Roe, H.G., 2019b. The mutual orbit, mass, and density of transneptunian binary G!kún||'hòmdímà (229762 2007 UK₁₂₆). Icarus (in press). https://doi.org/10.1016/j.icarus.2018.12.037.
- Harmon, J.K., Nolan, M.C., Giorgini, J.D., Howell, E.S., 2010. Radar observations of 8P/Tuttle: a contact-binary comet. Icarus 207, 499–502.
- Harris, A.W., Warner, B., 2018. Asteroid lightcurves: can't tell a contact binary from a brick. In: AAS/Division for Planetary Sciences Meeting No. 50, ID.414.03.
- Johansen, A., Youdin, A., Low, M.M., 2009. Particle clumping and planetesimal formation depend strongly on metallicity. Astrophys. J. 704, L75–L79.

References 223

- Johnston, W.R., 2018. Binary minor planets compilation C2.0 (PDS4). In: NASA Planetary Data System.
- Kominami, J.D., Makino, J., Daisaka, H., 2011. Binary formation in planetesimal disks I. Equal mass planetesimals. Publ. Astron. Soc. Jpn 63, 1331–1344.
- Kozai, Y., 1962. Secular perturbations of asteroids with high inclination and eccentricity. Astron. J. 67, 591–598.
- Lacerda, P., 2011. A change in the light curve of Kuiper belt contact binary (139775) 2001 QG₂₉₈. Astron. J. 142, 90.
- Lacerda, P., McNeill, A., Peixinho, N., 2014. The unusual Kuiper belt object 2003 SQ₃₁₇. Mon. Not. R. Astron. Soc. 437, 3824–3831.
- Leinhardt, Z.M., Marcus, R.A., Stewart, S.T., 2010. The formation of a collisional family around the dwarf planet Haumea. Astrophys. J. 714, 1789–1799.
- Levison, H.F., Stern, A.S., 2001. On the size dependence of the inclination distribution of the main Kuiper belt. Astron. J. 121, 1730–1735.
- Li, R., Youdin, A.N., Simon, J.B., 2018. On the numerical robustness of the streaming instability: particle concentration and gas dynamics in protoplanetary disks. Astrophys. J. 862, 14.
- Lidov, M.L., 1962. The evolution of orbits of artificial satellites of planets under the action of gravitational perturbations of external bodies. Planet. Space Sci. 9, 719–759.
- Margot, J.L., Brown, M.E., Trujillo, C.A., Sari, R., 2004. Hst observations of Kuiper belt binaries. Bull. Am. Astron. Soc. 36, 1081.
- Murray-Clay, R.A., Schlichting, H.E., 2011. Using Kuiper belt binaries to constrain Neptune's migration history. Astrophys. J. 730, 132.
- Naoz, S., Perets, H.B., Ragozzine, D., 2010. The observed orbital properties of binary minor planets. Astrophys. J. 719, 1775–1783.
- Nesvorný, D., Youdin, A.N., Richardson, D.C., 2010. Formation of Kuiper belt binaries by gravitational collapse. Astron. J. 140, 785–793.
- Nesvorný, D., Vokrouhlickyì, D., Bottke, W.F., Noll, K., Levison, H.F., 2011. Observed binary fraction sets limits on the extent of collisional grinding in the Kuiper belt. Astron. J. 141, 159.
- Nesvorný, D., Parker, J., Vokrouhlickyì, D., 2018. Bi-lobed shape of comet 67P from a collapsed binary. Astron. J. 155, 246.
- Noll, K.S., Stephens, D.C., Grundy, W.M., Griffin, I., 2004a. The orbit, mass, and Albedo of (66652) 1999 RZ₂₅₃. Icarus 172, 402–407.
- Noll, K.S., Stephens, D.C., Grundy, W.M., Osip, D., Griffin, I., 2004b. The orbit and Albedo of Trans-Neptunian binary (58534) 1997 CQ₂₉. Astron. J. 128, 2547–2552.
- Noll, K.S., Grundy, W.M., Chiang, E.I., Margot, J.L., Kern, S.D., 2008a. Binaries in the Kuiper belt. In: Barucci, M.A., Boehnhardt, H., Cruikshank, D.P., Morbidelli, A. (Eds.), The Solar System Beyond Neptune. University of Arizona Press, Tucson, AZ, pp. 345–363.
- Noll, K.S., Grundy, W.M., Stephens, D.C., Levison, H.F., Kern, S.D., 2008b. Evidence for two populations of classical transneptunian objects: the strong inclination dependence of classical binaries. Icarus 194, 758–768.
- Noll, K.S., Grundy, W.M., Schlichting, H.E., Murray-Clay, R.A., Benecchi, S.D., 2012. Resonant transneptunian binaries: evidence for slow migration of Neptune. In: AAS/Division for Planetary Sciences Meeting No. 44, ID.405.07.
- Noll, K.S., Parker, A.W., Grundy, W.M., 2014. All bright Cold Classicals are binary. In: AAS/Division for Planetary Sciences Meeting No. 46, ID.507.05.
- Osip, D.J., Kern, S.D., Elliot, J.L., 2003. Physical characterization of the binary Edgeworth-Kuiper belt object 2001 QT297. Earth Moon Planets 92, 409–421.
- Parker, A.H., Kavelaars, J.J., 2010. Destruction of binary minor planets during Neptune scattering. Astrophys. J. 722, L204–L208.
- Parker, A.H., Kavelaars, J.J., Petit, J.M., Jones, L., Gladman, B., Parker, J., 2011. Characterization of seven ultra-wide transneptunian binaries. Astrophys. J. 743, 1.
- Parker, A.H., Buie, M.W., Grundy, W.M., Noll, K.S., 2016. Discovery of a Makemakean moon. Astrophys. J. 825, L9.
- Peixinho, N., Delsanti, A., Doressoundiram, A., 2015. Reanalyzing the visible colors of Centaurs and KBOs: what is there and what we might be missing. Astron. Astrophys. 577, A35.
- Perets, H.B., Naoz, S., 2009. Kozai cycles, tidal friction, and the dynamical evolution of binary minor planets. Astrophys. J. 699, L17–L21.
- Porter, S.B., Grundy, W.M., 2012. KCTF evolution of Trans-Neptunian binaries: connecting formation to observation. Icarus 220, 947–957.

- Porter, S.B., Bierson, C.J., Umurhan, O., Beyer, R.A., Lauer, T.R., Buie, M.W., et al., 2019. A contact binary in the Kuiper belt: the shape and pole of (486958) 2014 MU₆₉. In: 50th Lunar and Planetary Science Conference, The Woodlands, Texas, ID 1611.
- Rabinowitz, D.L., Benecchi, S.D., Grundy, W.M., Thirouin, A., Verbiscer, A.J., 2016. Observations of mutual eclipses by the binary Kuiper belt object Manwë-Thorondor. In: AAS/Division for Planetary Sciences Meeting No. 48, ID.120.10.
- Ragozzine, D., Brown, M.E., 2009. Orbits and masses of the satellites of the dwarf planet Haumea (2003 EL₆₁). Astron. J. 137, 4766–4776.
- Ryan, E.L., Sharkey, B.N.L., Woodward, C.E., 2017. Trojan asteroids in the Kepler campaign 6 field. Astrophys. J. 153, 116.
- Schlichting, H.E., Sari, R., 2008. The ratio of retrograde to prograde orbits: a test for Kuiper belt binary formation theories. Astrophys. J. 686, 741–747.
- Sheppard, S.S., Jewitt, D., 2004. Extreme Kuiper belt object 2001 QG₂₉₈ and the fraction of contact binaries. Astrophys. J. 127, 3023–3033.
- Sheppard, S.S., Ragozzine, D., Trujillo, C., 2012. 2007 TY₄₃₀: a cold classical Kuiper belt type binary in the Plutino population. Astron. J. 143, 58.1-13.
- Sickafoose, A.A., Bosh, A.S., Levine, S.E., Zuluaga, C.A., Genade, A., Schindler, K., et al., 2019. A stellar occultation by Vanth, a satellite of (90482) Orcus. Icarus 319, 657–668.
- Simon, J.B., Armitage, P.J., Youdin, A.N., Li, R., 2017. Evidence for Universality in the initial planetesimal mass function. Astrophys. J. 847, L12.
- Stansberry, J.A., Grundy, W.M., Brown, M.E., Cruikshank, D.P., Spencer, J.R., Trilling, D.E., et al., 2008. Physical properties of Kuiper belt and centaur objects: constraints from the Spitzer Space Telescope. In: Barucci, M.A., Boehnhardt, H., Cruikshank, D.P., Morbidelli, A. (Eds.), The Solar System Beyond Neptune. University of Arizona Press, Tucson, AZ, pp. 161–179.
- Stansberry, J.A., Grundy, W.M., Mueller, M., Benecchi, S.D., Rieke, G.H., Noll, K.S., Buie, M.W., Levison, H.F., Porter, S.B., Roe, H.G., 2012. Physical properties of transneptunian binaries (120347) Salacia-Actaea and (42355) Typhon-Echidna. Icarus 219, 676–688.
- Stephens, D.C., Noll, K.S., 2006. Detection of six trans-Neptunian binaries with NICMOS: a high fraction of binaries in the cold classical disk. Astron. J. 131 (2), 1142–1148.
- Tegler, S., Romanishin, W., 2000. Extremely red Kuiper-belt objects in near-circular orbits beyond 40 AU. Nature 407, 979–981.
- Thirouin, A., Sheppard, S.S., 2017. A possible dynamically cold classical contact binary: (126719) 2002 CC₂₄₉. Astron. J. 154, 241.
- Thirouin, A., Sheppard, S.S., 2018. The Plutino population: an abundance of contact binaries. Astron. J. 155, 248.
- Thirouin, A., Sheppard, S.S., 2019. Lightcurves and rotational properties of the pristine cold classical Kuiper belt objects. Astron. J. (submitted).
- Thirouin, A., Sheppard, S.S., Noll, K.S., 2017. 2004 TT₃₅₇: a potential contact binary in the Trans-Neptunian belt. Astrophys. J. 844, 135.
- Thirouin, A., Noll, K.S., Ortiz, J.L., Morales, N., 2014. Rotational properties of the binary and non-binary populations in the Trans-Neptunian belt. Astron. Astrophys. 569, A3.
- Veillet, C., Parker, J.W., Griffin, I., Marsden, B., Doressoundiram, A., Buie, M., Tholen, D.J., Connelley, M., Holman, M.J., 2002. The binary Kuiper-belt object 1998 WW₃₁. Nature 416, 711–713.
- Vilenius, E., Kiss, C., Mommert, M., Müller, T., Santos-Sanz, P., Pal, A., et al., 2012. "TNOs are Cool": a survey of the Trans-Neptunian region. VI. Herschel/PACS observations and thermal modeling of 19 classical Kuiper belt objects. Astron. Astrophys. 541, A94.1-17.
- Vilenius, E., Kiss, C., Müller, T., Mommert, M., Santos-Sanz, P., Pal, A., et al., 2014. "TNOs are Cool": a survey of the Trans-Neptunian region X. Analysis of classical Kuiper belt objects from Herschel and Spitzer observations. Astron. Astrophys. 564, A35.1-18.
- Youdin, A.N., Goodman, J., 2005. Streaming instabilities in protoplanetary disks. Astrophys. J. 620, 459–469.

Further reading

Parker, A.H., Kavelaars, J.J., 2012. Collisional evolution of ultra-wide transneptunian binaries. Astrophys. J. 744, 139.1-14.